Dissociative electron attachment to HCN and HNC

S. T. Chourou[*] and A. E. Orel

Department of Applied Science, University of California, Davis, California 95616, USA

Previous experimental and theoretical studies on HCN and HNC have indicated the presence of both σ and π low-lying shape resonances. The energy and autoionization width of these resonant states depend on the stretching and bending of the molecule and lead primarily to a $(CN^- + H)$ product. In this work, we present a comparative study of the dissociation mechanism of these isomers. We carried out electron scattering calculations using the complex-Kohn variational method as a function of the three internal degrees of freedom to obtain the resonance energy surfaces and autoionization widths. We then use these data as input to form the Hamiltonian relevant to the nuclear dynamics. The multidimensional wave equation is solved using the multiconfiguration time-dependent Hartree approach. We compute the relative dissociative electron attachment cross sections and examine the isotope effect relative to each isomer.

I. INTRODUCTION

Studies on the interstellar formation of hydrogen cyanide and hydrogen isocyanide have shown that the process involves electron driven chemistry on H_2CN^+ as demonstrated by Conrad and Schaefer III in [1] and the references therein. The authors believe that the three isomers of H_2CN^+ play a role in the production of HCN and HNC in both dense and diffuse interstellar clouds. A dissociative recombination reaction to H_2CN^+ has been postulated to explain the relative abundance [HCN]/[HNC] in these media which is of relevance to the astrophysics community.

Gupta *et al.* studied evolution mechanisms in the atmosphere of Titan where HCN and certain derivatives such as cyanopolyacetylene have been detected and are believed to be precursors to biologically important species [2]. Moreover, it has been shown that the decrease in temperature in upper atmosphere of Titan correlates with a considerably higher abundance of HCN [3]. The importance of HCN as an initial compound that drives the abiotic synthesis of complex organic molecules in gaseous media has further been reported [4]. Investigation of the effects of electron impact on HCN and HNC is thus crucial to understand the overall chemistry governing these environments.

HCN has been studied extensively in the literature, however, studies of electron collisions with HCN and of the negative ions, HCN^- and HNC^-, remain rather limited. Early experiments on dissociative attachment to HCN by Inoue *et al.* revealed a peak of CN^- anion yield situated around 2.5 eV of electron collision energy [5]. Later, measurements by Burrow *et al.* using electron transmission spectroscopy of HCN displayed pronounced resonances at 2.26 eV which was attributed to electron capture into the doubly degenerate π^* orbital [6].
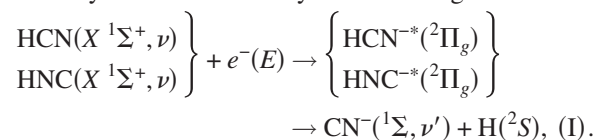
Calculations by Jain and Norcross located the π^*-shape resonance energy at 2.71 eV with a width of 1.9 eV at the equilibrium geometry of HCN [7]. The authors carried out calculations involving the stretching of $C\equiv N$ and $C-H$

bonds as well as bending of the molecule and reported significant dependence on potential energy on these degrees of freedom [8]. They observed the intersection of the $^2\Pi$ anion state with the neutral HCN curve occurring at 2.9 a.u. $C\equiv N$ bond distance and the appearance of a broad σ^* shape resonance when the $C\equiv N$ or $C-H$ bond is stretched far enough from equilibrium. These effects are expected to play a role in the dissociation dynamics of the molecular anion.

In addition, Edard *et al.* reported measurements of the vibrational excitation of HCN following the decay of the low-lying π and σ resonances which were found to lie at 2.3 and 6.7 eV, respectively [9]. The authors observed strong $C\equiv N$ stretch activity accompanied by bending vibrations, consistent with electron trapping into a π^* orbital.

More recently, Varambhia and Tennyson applied the *R*-matrix method to study electron scattering from HCN and HNC [10]. They observed both a π^* resonance ranging between 2.46 and 3.27 eV with a width ranging between 1.14 and 1.64 eV depending on the model used while no resonance feature in Σ symmetry seems to be present for HCN. In the case of HNC, calculations revealed similar positions for resonance energies (lying between 2.57 and 3.03 eV) and narrower autodetachment widths (between 0.67 and 1.1 eV) in Π symmetry, while a σ^* appears in the 8 eV region with a width up to three orders of magnitude narrower than its π^* counterpart.

The present work focuses on the dissociative electron attachment (DEA) process (I) leading the formation of CN^-. We provide a full description of reaction dynamics and computation of the relative DEA cross section from selected initial vibrational states ν of HCN and HNC. The process of interest may be summarized by the following reaction:

$$\left. \begin{array}{l} HCN(X\,^1\Sigma^+, \nu) \\ HNC(X\,^1\Sigma^+, \nu) \end{array} \right\} + e^-(E) \rightarrow \left\{ \begin{array}{l} HCN^{-*}(^2\Pi_g) \\ HNC^{-*}(^2\Pi_g) \end{array} \right\}$$
$$\rightarrow CN^-(^1\Sigma, \nu') + H(^2S),\ (I).$$

In this paper, we present the theoretical approach and the computational techniques we used to calculate the adiabatic potential energy surfaces (APESs) associated with the ground electronic state of the neutral HCN/HNC target. In

---

*stchourou@ucdavis.edu

Sec. II, we further describe the electron scattering calculation performed to determine the resonant states and construct the complex APES used in the computation of the nuclear dynamics of HCN^{-*}/HNC^{-*}. In Sec. IV, we present the potential energy structure, report the DEA cross section of each of the two isomers, and address the associated isotope effect.

II. *AB INITIO* METHODS

A. Target description

We seek to construct the APES relevant to the initial electronic state of the molecule as a function of its internal degrees of freedom. In order to include the initial vibrational states of both HCN and HNC neutral targets, we perform calculations that include the full bending range of the molecule that lead to the isomerization of the molecule.

In this study, we perform electronic structure calculation using the multiconfiguration self-consistent field approach followed by a multireference configuration interaction (MRCI) calculation for various geometries of the molecule.

The carbon, nitrogen, and hydrogen atoms were described using a triple-zeta-plus-polarization function basis set which is then augmented with s and p diffuse orbitals as follows: three s functions with exponents 0.05, 0.02, and 0.003 centered on the carbon, three s functions with exponents 0.07, 0.02, and 0.003 centered on the nitrogen, and two s functions with exponents 0.03 and 0.01 and two p functions with exponents 0.06 and 0.02 centered on the hydrogen. The MRCI calculation is carried out by freezing four core electrons and including single excitations in an active space of 52 molecular orbitals.

B. Resonances

Low energy electron collision with the neutral target leads to formation of a transient negative ion state resulting from the temporary trapping of the incident electron by the molecular centrifugal barrier into a shape resonance. Since this state is embedded in the continuum, we perform electron scattering calculations to determine both the resonance energies ϵ_{res} and the autoionization widths Γ as a function of the molecule internal coordinates.

We use the complex-Kohn variational method [11] where in a first approximation (static exchange level), we neglect the polarization and correlation effects so that the $(n+1)$-electron scattering wave function for fixed nuclei positions represented collectively by the vector **Q** reduces to

$$\varphi_{el}^{\lambda}(\mathbf{r}^{n+1};\mathbf{Q}) = \hat{A}\left[\sum_{\lambda'}\phi_{el}^{\lambda}(\mathbf{r}^n;\mathbf{Q})F^{\lambda\lambda'}(\vec{r}_{n+1};k)\right], \qquad (1)$$

where $\mathbf{r}^{n+1}=(\vec{r}_1,\vec{r}_2,\ldots,\vec{r}_{n+1})$ is the $(n+1)$-electronic coordinate vector and $\hat{A}$ is the antisymmetrizing operator. The function $\phi_{el}^{\lambda}(\mathbf{r}^n;\mathbf{Q})$ is the target n-electron ground state in the irreducible representation λ with the nuclei clamped at **Q**. $F^{\lambda\lambda'}(\vec{r}_{n+1};k)$ is the scattering electron's wave function at position $\vec{r}$ and momentum k, which is further expanded to match asymptotic boundary conditions,
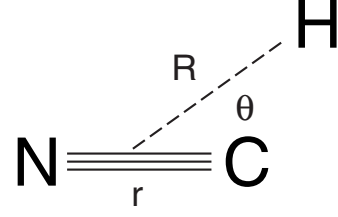

FIG. 1. Molecule in Jacobi coordinates. The hydrogen undergoes bending from the HCN geometry ($\theta=0°$) to the HNC geometry ($\theta=180°$).

$$F^{\lambda\lambda'}(\vec{r};k) = \sum_i c_i^{\lambda\lambda'} u_i(\vec{r}) + \sum_{lm}\left[f_l^{\lambda}(kr)\delta_{ll'}\delta_{mm'}\delta_{\lambda\lambda'}\right.$$
$$\left. + T_{ll'mm'}^{\lambda\lambda'}(k)h_l^{+\lambda}(kr)\right]Y_{lm}(\hat{r})/r, \qquad (2)$$

where the $\{u_i\}_i$ are square-integrable functions, $\{f_l^{\lambda}\}_l$ and $\{h_l^{+\lambda}\}_l$ are the regular Ricatti-Bessel and the outgoing Hankel functions, respectively, and Y_{lm} are the normalized spherical harmonics. The terms $T_{ll'mm'}^{\lambda\lambda'}$ are the T-matrix elements that determine the eigenphase sums as a function of the electron's collision energy. By fitting the eigenphase sums to the Breit-Wigner form, we determine the resonance parameters ϵ_{res}^{λ} and Γ^{λ}.

C. Nuclear dynamics

We solve for the nuclear dynamics of the metastable negative ion state in the local complex potential model. The approximation used in this model has been discussed in detail elsewhere [12] and will only be outlined here. The nuclear wave equation is given by

$$[E_{tot} - \hat{H}(\mathbf{Q})]\xi_{nuc}^{\Lambda}(\mathbf{Q}) = \eta_{\nu}^{\Lambda}(\mathbf{Q}), \qquad (3)$$

where the Hamiltonian operator is given by

$$\hat{H}(\mathbf{Q}) = \hat{T}_Q + V_{el}^{\lambda}(\mathbf{Q}). \qquad (4)$$

Here, the superscript Λ represents the irreducible representation relevant to the nuclear wave functions. We have chosen to express the system in Jacobi coordinates $\mathbf{Q}=(r,R,\theta)$, as shown in Fig. 1. The kinetic energy operator $\hat{T}_Q$ for a total momentum operator $J=0$ is given by

$$\hat{T}_Q = -\frac{1}{2\mu_r}\partial_r^2 - \frac{1}{2\mu_R}\partial_R^2 - \frac{1}{2}\left(\frac{1}{\mu_r r^2} + \frac{1}{\mu_R R^2}\right)\frac{1}{\sin\theta}\partial_\theta(\sin\theta\,\partial_\theta),$$
$$(5)$$

where μ_r and μ_R specify the reduced masses associated with the r and R coordinates. (Note that we use atomic units $\hbar=m=1$ throughout.) The complex potential $V_{el}^{\lambda}(\mathbf{Q})$ relevant to the resonant HCN^{-*} anion is defined by

$$V_{el}^{\lambda}(\mathbf{Q}) = E_{el}^{\lambda}(\mathbf{Q}) + \epsilon_{res}^{\lambda}(\mathbf{Q}) - \frac{i}{2}\Gamma^{\lambda}(\mathbf{Q}). \qquad (6)$$

The driving term $\eta_{\nu}^{\Lambda}(\mathbf{Q})$ in Eq. (3) is known as the "entry amplitude" and it expresses the capture probability of the incoming electron by the molecular target in the discrete vi-

brational state $\chi_\nu^\Lambda(\mathbf{Q})$ into the resonant state associated with the complex potential of Eq. (6). In our model, it is expressed as

$$\eta_\nu^\Lambda(\mathbf{Q}) = \left(\frac{\Gamma^\Lambda(\mathbf{Q})}{2\pi}\right)^{1/2} \chi_\nu^\Lambda(\mathbf{Q}). \qquad (7)$$

Finally, $\xi_{nuc}^\Lambda(\mathbf{Q})$ is the nuclear wave function we seek to determine. We use the time-dependent formulation established by McCurdy and Turner [13]. The problem thus reduces to solving the time-dependent Schrödinger equation,

$$\hat{H}(\mathbf{Q})\Phi_{nuc}^\Lambda(\mathbf{Q},t) = i\partial_t \Phi_{nuc}^\Lambda(\mathbf{Q},t),$$

$$\Phi_{nuc}^\Lambda(\mathbf{Q},0) = \eta_\nu^\Lambda(\mathbf{Q}). \qquad (8)$$

We use the computational technique based on multiconfiguration time-dependent Hartree (MCTDH) formalism discussed in detail in [14]. In the context of this theory, the nuclear wave function for the negative ion of HCN is expressed in the Jacobi coordinates as

$$\Phi_{nuc}^\Lambda(r,R,\theta,t) = \sum_{i=1}^{N_r}\sum_{j=1}^{N_R}\sum_{k=1}^{N_\theta} A_{ijk}(t)\rho_i(r,t)\varrho_j(R,t)\Theta_k(\theta,t). \qquad (9)$$

Each single-particle function appearing in Eq. (9) is in turn expanded in terms of a function basis set chosen to correspond to that of a discrete variable representation (DVR) for computational efficiency. Here, N_r, N_R, and N_θ are all set to the value 8 and the single-particle functions associated with the variables R, r, and θ are expressed in terms of sine-DVR (99 grid points), harmonic oscillator-DVR (27 grid points), and Legendre-DVR (121 grid points), respectively.

III. COMPUTATIONAL RESULTS

In its electronic ground state, both HCN and HNC have linear geometry and belong to the $C_{\infty v}$ point group. The electronic structure calculation provides the molecular orbital structure, hence, the electronic configuration of the ground state

$$(X\ {}^1\Sigma^+)1\sigma^2 2\sigma^2 3\sigma^2 4\sigma^2 5\sigma^2 1\pi^4.$$

Since we address the DEA channel described by (I) involving the motion and breakup of the hydrogen atom, the Jacobi coordinates shown in Fig. 1 are a suitable choice for describing the geometry of the system. The coordinate R represents the distance between H and the center of mass G of C≡N and θ represents the angle between C≡N and H−G. Therefore, our calculations will include the three internal degrees of freedom where the molecular grid is defined within the domain $r \in [1.9 \text{ a.u.}, 3.2 \text{ a.u.}]$, $R \in [2.1 \text{ a.u.}, 7.0 \text{ a.u.}]$, and $\theta \in [0°, 180°]$.

A. Neutral APES

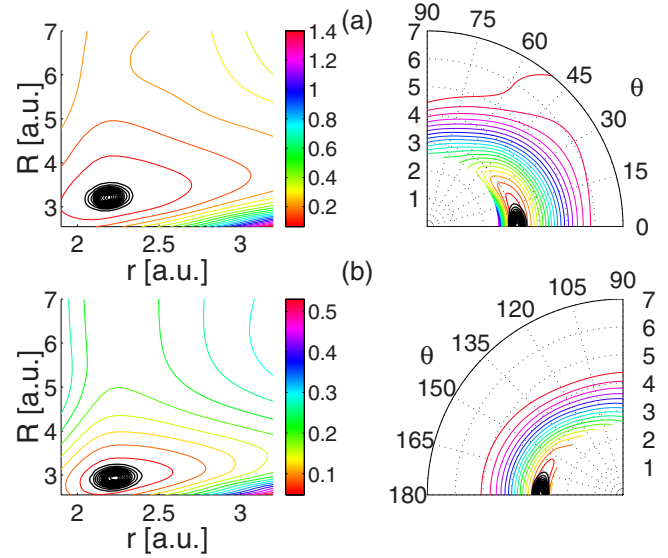The ground potential energy surface of HCN and HNC is shown in Fig. 2 and shows two minima at each linear geom-

FIG. 2. (Color online) Potential energy surfaces of the ground state of the neutral HCN (first row) and HNC (second row) as a function of r and R and R and θ (color-scale contours). Black contours represent the ground vibrational state.

etry lying at $(r_{eq}=2.19 \text{ a.u.}, R_{eq}=3.22 \text{ a.u.})$ and $(r_{eq}=2.23 \text{ a.u.}, R_{eq}=2.94 \text{ a.u.})$, respectively, for HCN and HNC where the energy for HCN lies about 0.02 a.u. (0.54 eV) lower than its HNC counterpart, in agreement with previous studies [15]. The dissociation energy is found to be 0.2 a.u. (5.44 eV) for HCN and 0.18 a.u. (4.98 eV) for HNC. Furthermore, the asymptotic negative ion curve lies about 0.14 a.u. (3.80 eV) below the neutral consistently with the C≡N electron affinity of 3.82 ± 0.02 eV found in [16].

B. Resonant APES

The computation of the eigenphase sums as a function of incident electron energy reveals two low-lying shape resonances. In Figs. 3 and 4, the eigenphase plots show the resonance features of HCN and HNC in A' symmetry up to an electron collision energy of 0.5 a.u. (13.61 eV). Figure 3(a) [Fig. 3(b)] displays the effect of the stretching the hydrogen bond while maintaining a small bending angle $\theta=1°$ ($\theta=179°$) from the linear geometry of HCN (HNC). The main resonance feature occurring between 0.1 and 0.2 a.u. (2.72 and 5.44 eV) remains practically unchanged under stretching of the hydrogen bond. This implies a nondissociative process if the molecule is restrained to be linear.

Figure 4(a) [Fig. 4(b)] depicts the effect of HCN (HNC) bending from linearity while keeping a constant value for $R=3.22$ a.u. in A' symmetry. In quasilinear geometry (1° bend), the two A' resonances are overlapping. By increasing the bending angle, we observe the position of one of the resonance approaching thresholds while narrowing in width. This indicates that a dissociative channel may open if the bending coordinate is taken into account.

We have used a function fitting procedure based on a superposition of two Breit-Wigner forms in order to get an approximation of the resonance parameters of the two reso-
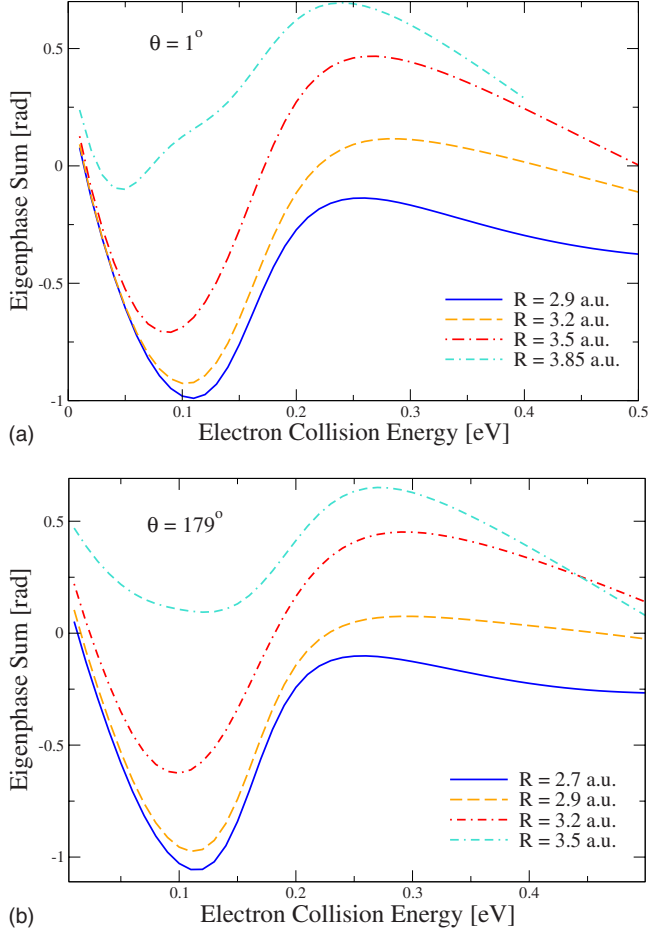
FIG. 3. (Color online) (a) Stretching effect of the hydrogen bond on the eigenphase sums in A' symmetry where the molecule is at $\theta = 1°$ bend. (b) Stretching effect of the hydrogen bond on the eigenphase sums in A' symmetry where the molecule is at $\theta = 179°$ bend. The resonance feature between 0.1 and 0.2 a.u. does not undergo a change in position or width with stretching in both cases.

FIG. 4. (Color online) Molecule bending effect on the eigenphase sums in A' symmetry for $R = 3.22$ a.u. in the case of (a) HCN and (b) HNC. The resonance feature converges toward threshold and "sharpens" with bending in both cases.

nant states. The function expression used is given by

$$\delta_{sum}\left(\frac{k^2}{2}\right) = \sum_{p=1}^{2} \arctan\left(\frac{\Gamma_p^{A'}/2}{\epsilon_{res,p}^{A'} - \frac{k^2}{2}}\right) + \delta_{bkgd}\left(\frac{k^2}{2}\right), \quad (10)$$

where $(\epsilon_{res,p}^{A'}, \Gamma_p^{A'})$ are the corresponding parameters to be determined and δ_{bkgd} is the background phase shift taken to be a slowly varying function of the electron energy.

By iterating this procedure over the various grid points we construct the resonant surfaces where cuts along the dissociating coordinate are shown in Figs. 5 and 6. We observe a curve crossing between the $^2\Sigma$ and $^2\Pi$ states in linear geometry for both HCN and HNC. By bending the molecule, the degeneracy of the $^2\Pi$ state is lifted and the lower manifold $1\,^2A'$ presents a barrier with decreasing height as the molecule is bent in the case of the two isomers. This barrier is broader and about 0.035 a.u. (0.95 eV) higher at its maximum for HNC than for HCN. This forms a conical intersection similar to the structure found in the case of the isoelectronic acetylene molecule in [17].
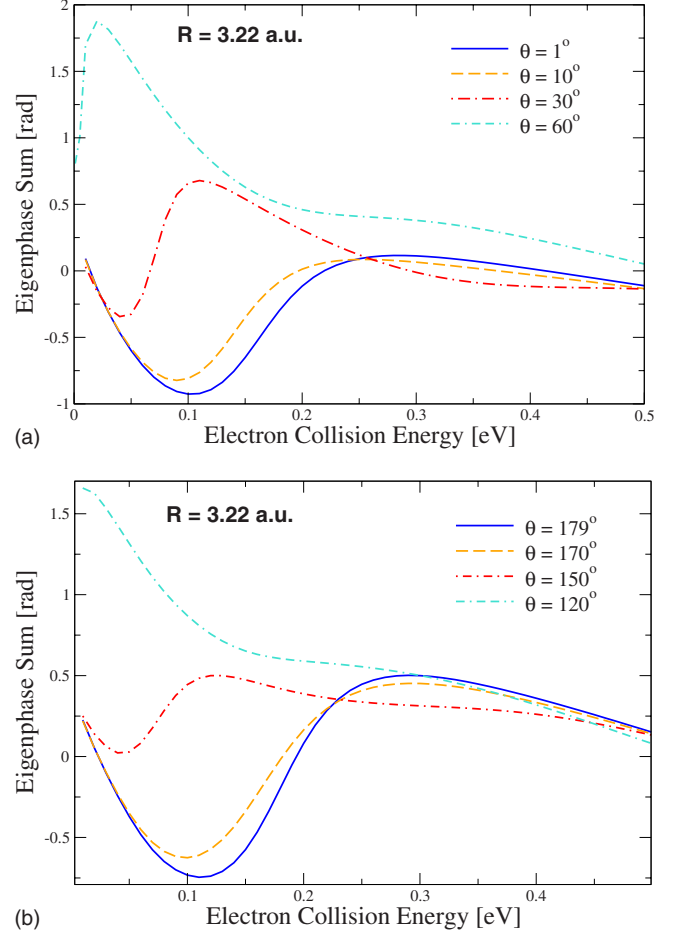
C. Nuclear dynamics

The wave packet for the ground neutral state is computed by relaxation on the neutral APES and is shown in Fig. 2. By applying Eq. (7), we determine the initial wave packet needed to solve the system of equation [Eq. (8)]. In this study, we consider propagation on the $1\,^2A'$ manifold; considerations of APES interactions and nonadiabatic effects are beyond the scope of the present paper. Thus, in Eq. (4), the potential is given by $E_{el}^{1\,^2A'}(\mathbf{Q}) + \epsilon_{res}^{1\,^2A'}(\mathbf{Q}) - \frac{i}{2}\Gamma^{1\,^2A'}(\mathbf{Q})$.

At the grid boundaries, an appropriate complex absorbing potential (CAP) is included to ensure that wave packet is not reflected back into the grid causing undesired interferences. The form of the CAPs adopted in this study is given by the form

$$-iW(R) = -iC|R - R_{CAP}|^b S(R - R_{CAP}), \quad (11)$$

where S is the Heaviside step function and the values of the parameters C, b, and R_{CAP} used in this propagation are 0.09, 2, and 6.0 a.u., respectively. Propagation is carried out for a duration of 20 fs. In the plots of Fig. 7, we observe that the initial wave packet travels in the direction of increasing R and θ. This indicates that the molecule's angular vibrational
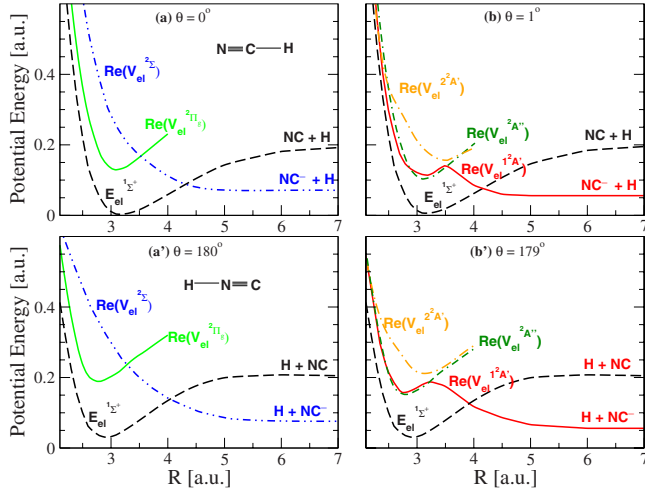
FIG. 5. (Color online) Potential energy curves in (a) linear (θ =0°) and (b) quasilinear (θ=1°) geometries. Plots in (a) and (a') show the curve crossing between $^2\Sigma$ (dotted-dotted-dashed line) and $^2\Pi$ (solid line) states. Plots in (b) and (b') show the lifting of the degeneracy of $^2\Pi$ state and splitting into the 1 $^2A'$ (solid line) and 2 $^2A'$ (dotted-dashed line) adiabatic manifolds. The shape of the $^2A''$ manifold (dotted-dotted-dashed line) does not vary with bending.

modes are excited as the hydrogen atom dissociates. We further note that the bending is more predominant in the case of HCN where we observe a more pronounced spreading along the angular dimension than in the case of HNC. The HCN dissociation dynamics is dominated by a tunneling effect through 1 $^2A'$ barrier causing the process to be faster than its

HNC counterpart where the wave packet undergoes more oscillations along the r and θ coordinates. Since the complex potential is characterized by a negative imaginary part, the HNC wave packet is more significantly damped leading to lower flux. This is expected to lead to a lower total cross section for DEA in HNC$^-$.

D. Cross section

The wave packet flux at the grid boundaries is used to compute the DEA cross section. The energy-resolved outgoing flux associated with the initial target vibrational state ν through the CAP is therefore given by

$$F_\nu^{(I)}(E) = \frac{1}{(2\pi)^2 |\Delta(E)|^2} \langle \xi_\nu^\Lambda | \hat{F}^{(I)} | \xi_\nu^\Lambda \rangle_\mathbf{Q}, \quad (12)$$

where $\hat{F}^{(I)}$ is the flux operator. In order to achieve a time-dependent dynamics formulation of the process, the bracket term in Eq. (12) is computed in terms of the time domain integrals as

$$\langle \xi_\nu^\Lambda | \hat{F}^{(I)} | \xi_\nu^\Lambda \rangle_\mathbf{Q} = \int_0^\infty dt \int_0^\infty dt' \langle \eta_\nu^\Lambda | e^{i(\hat{\tilde{H}}^\dagger - E)t} \hat{F}^{(I)} e^{-i(\hat{\tilde{H}} - E)t'} | \eta_\nu^\Lambda \rangle_\mathbf{Q},$$

$$(13)$$

where the operator $\hat{\tilde{H}}$ is given by

$$\hat{\tilde{H}} = \hat{H} - iW(R), \quad (14)$$

representing the CAP-perturbed Hamiltonian of the system defined in Eq. (4). The cross section relevant to the DEA
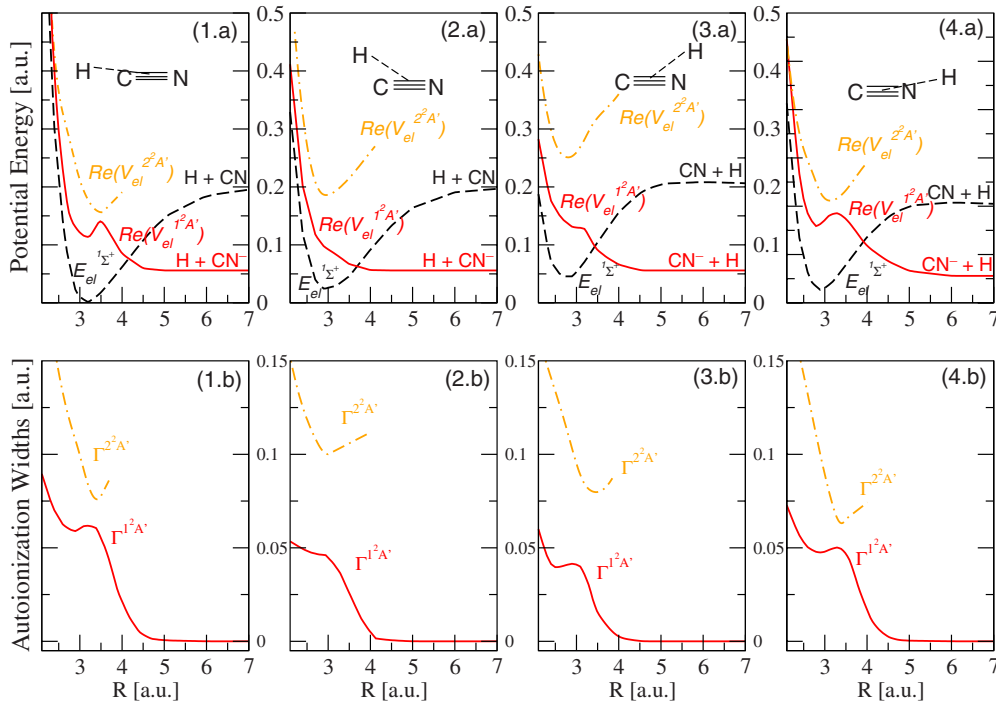

FIG. 6. (Color online) Effect of bending the hydrogen in the molecule from HCN to HNC geometry. The upper row shows cuts of the APES along R for θ=1°, 30°, 150°, and 180° in panels (1.a), (2.a), (3.a), and (4.a), respectively. The lower row shows the corresponding imaginary part of the complex potential.
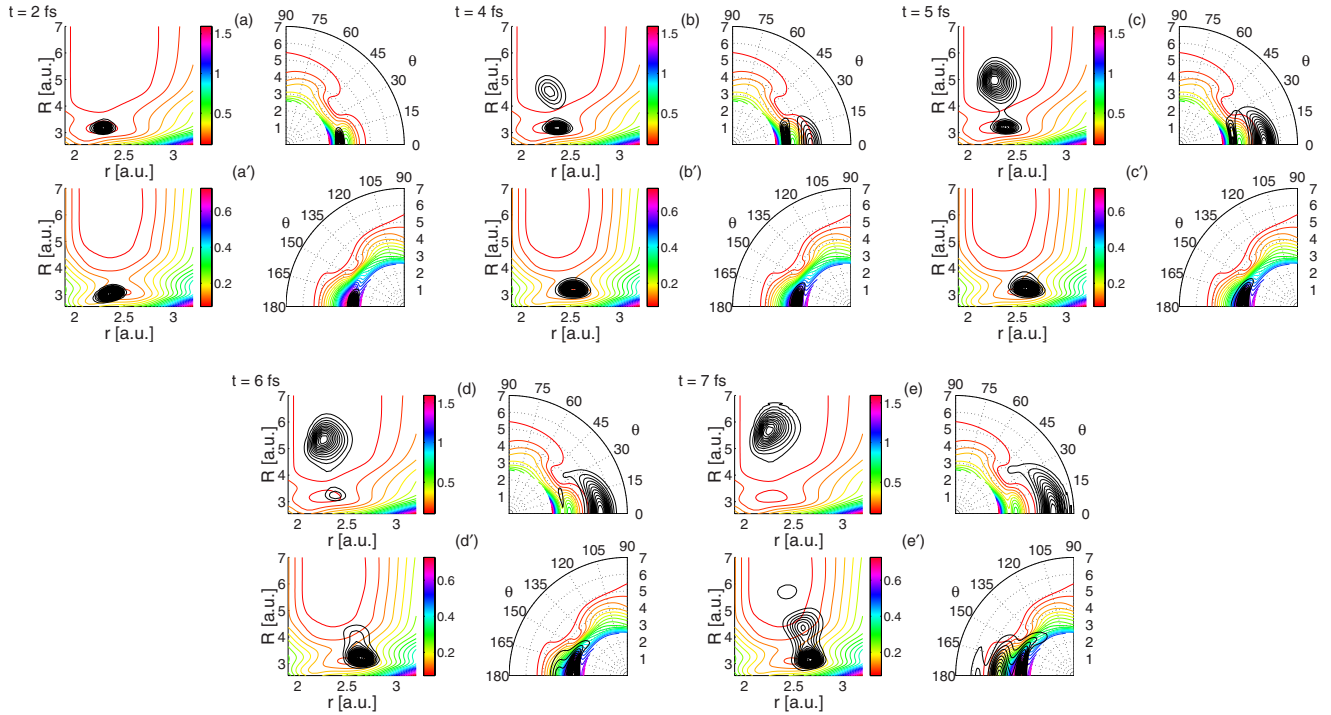
FIG. 7. (Color online) Snapshots of the wave packet (black contours) propagation on the $V_{el}^{1A'}(r,R,\theta)$ APES (color-scale contours) taken at 2, 4, 5, 6, and 7 fs. The left panels show the propagation on a (R,r) grid (wave packet integrated over the θ coordinate) and the right panels show the propagation on a (R,θ) polar grid (wave packet integrated over the r coordinate). The (a), (b), (c), (d), and (e) snapshots are associated with DEA to HCN whereas (a′), (b′), (c′), (d′), and (e′) are associated with DEA to HNC.

channel (I) for an initial neutral target in the vibrational mode ν may be expressed based on the flux function as

$$\sigma_{\nu \to \mathrm{DEA}}\left(\frac{k^2}{2}\right) = g_s g_a \frac{4\pi^3}{k^2} F_\nu^{(I)}\left(\frac{k^2}{2}\right), \tag{15}$$

where g_s is the statistical ratio of the electronic multiplicity of the resonant state to the electron multiplicity of the neutral target (here equal to 2) and g_a is the arrangement multiplicity (here equal to 1). The reader is referred to Refs. [18–21] for detailed treatment of the CAP-based flux formalism.

We compute the individual DEA cross sections for an initial target vibrational mode, then calculate the population-weighted sum using Boltzmann factors at 300 K. For HCN, the frequencies for CH and CN σ^+-stretching modes are 3311 cm^{-1} (0.41 eV) and 2097 cm^{-1} (0.26 eV), respectively, and the frequency for the π-bending mode is 712 cm^{-1} (0.08 eV) [22]. As for HNC, the frequencies for NH and NC σ^+-stretching modes are 3643 cm^{-1} (0.45 eV) and 2025 cm^{-1} (0.25 eV), respectively [23], whereas the frequency for the π-bending mode is 477 cm^{-1} (0.06 eV) [24]. For a temperature of 300 K only the ground vibrational state in the two stretch modes is significantly populated. However, since the bending frequency is at least three times smaller than the stretching frequencies for both isomers, we must include contributions of the three first bending modes. The excited states are obtained by applying successively an angular raising operator on the ground vibrational mode.

The resulting DEA cross section for $\nu=0$, 1, and 2 as well as the population-weighted sum at 300 K are shown in Figs.

8(a) and 8(b), respectively, for HCN and HNC. We obtain a peak around 3 eV for both isomers and a peak height of 2.8×10^{-17} cm^2 for HCN and 1.03×10^{-17} cm^2 for HNC. Therefore, the DEA cross section ratio $\sigma_{\mathrm{DEA}}(\mathrm{CN}^-, \mathrm{HCN})/\sigma_{\mathrm{DEA}}(\mathrm{CN}^-, \mathrm{HNC})$ is of the order of 2.7. This rather significant ratio may be attributed to the broader potential barrier shown for HNC causing the tunneling probability to be lower. Furthermore, the cross section plots imply that the contribution of the vibrationally excited bending modes is not substantial for both isomers at 300 K which confirms the limited role of molecular bending in the production of CN$^-$ ions in the 3 eV energy range. This is in contrast to the case of acetylene [25], where bending enhanced the DEA cross section. The dissociation in these systems proceeds predominately via tunneling through the barrier (see Fig. 7) rather than a reaction path that bends to avoid the barrier. This is similar to what was seen in our studies of ClCN and BrCN [26], where bending was much less important in the dissociation.

E. Isotope effect

We carried out dynamics calculations on the deuterated targets, DCN and DNC, to investigate the isotope effect in DEA to hydrogen cyanide and its isomer. We applied the same techniques used for obtaining the individual vibrational state cross sections, then performing a population-weighted sum using Boltzmann factors at 300 K. The results for the ground state, first and second angular vibrational modes, are shown in Figs. 9(a) and 9(b), respectively, for DCN and
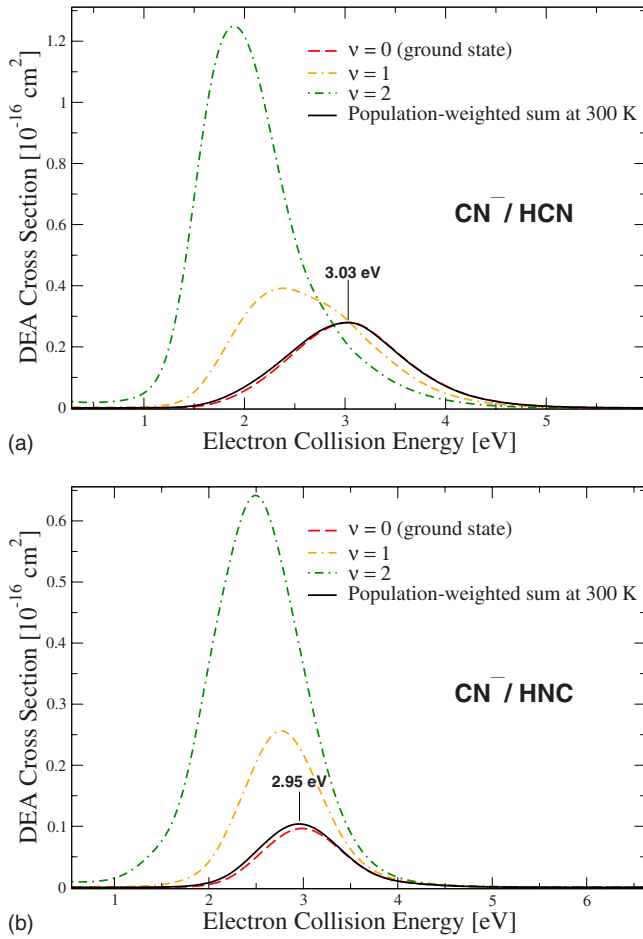
FIG. 8. (Color online) DEA cross section for CN^- production from (a) HCN and (b) HNC for individual low-lying angular vibrational states (nonsolid lines) and the population-weighted sum at 300 K (solid line).
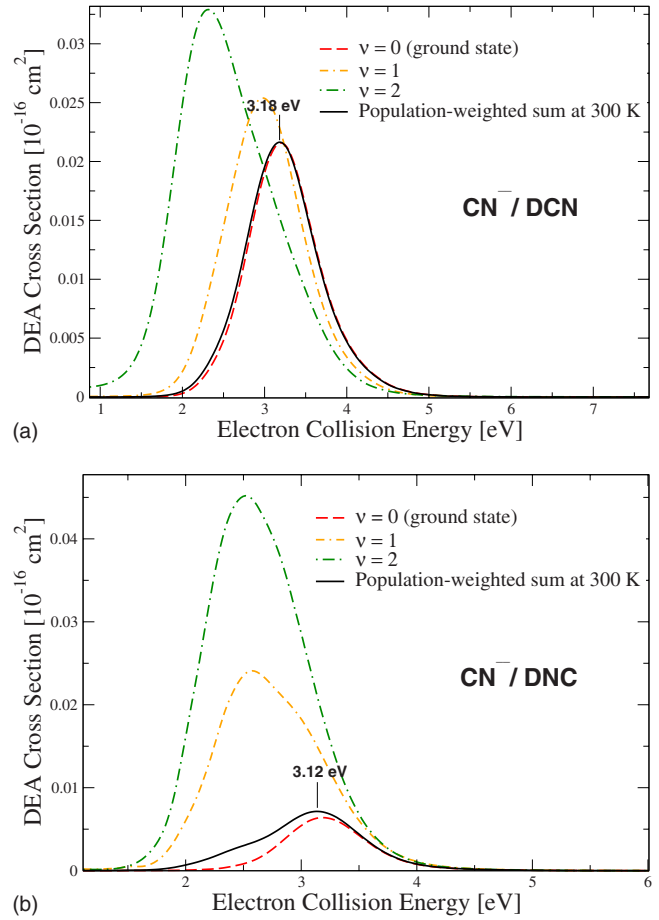

FIG. 9. (Color online) DEA cross section for CN^- production from (a) DCN and (b) DNC for individual low-lying angular vibrational states (nonsolid lines) and the population-weighted sum at 300 K (solid line).

DNC. We obtain a $\sigma_{DEA}(CN^-, HCN)/\sigma_{DEA}(CN^-, DCN)$ ratio of 13 and a $\sigma_{DEA}(CN^-, HCN)/\sigma_{DEA}(CN^-, DCN)$ ratio of 14.6 approximately. This isotope effect is comparable to that observed in the case of the isoelectronic acetylene [27]. The relatively low anion yield in the case of DNC may be attributed to a weaker tunneling effect in the dissociation dynamics of the deuterium for this isomer.

IV. CONCLUSION

We have carried out theoretical calculations on DEA in the two isomers, HCN and HNC, in order to understand the mechanisms for dissociation in these systems. Our calculations show several resonances that in linear geometry correspond to σ^* and π^* shape resonances. In linear geometry

there is a barrier to dissociation that is lowered when bending is included. The dynamics proceeds, predominately, via tunneling through the barrier with bending playing a limited role. HNC is found to have a lower DEA cross section compared to HCN. The isotope effect is similar to what is seen in acetylene, but the effect of initial excitation in the bending mode is less, supporting the tunneling mechanism.

ACKNOWLEDGMENTS

[1] M. P. Conrad and H. F. Schaefer III, Nature (London) **274**, 456 (1978).

[2] S. Gupta, E. Ochiai, and C. Ponnamperuma, Nature (London) **293**, 725 (1981).

[3] R. V. Yelle, Astrophys. J. **383**, 380 (1991).

[4] S. Yuasa, D. Flory, B. Basile, and J. Oro, J. Mol. Evol. **20**, 52 (1984).

[5] M. Inoue, J. Chim. Phys. Phys.-Chim. Biol. **63**, 1061 (1966).

[6] P. D. Burrow, A. E. Howard, A. R. Johnston, and K. D. Jordan, J. Phys. Chem. **96**, 7570 (1992).

[7] A. Jain and D. W. Norcross, Phys. Rev. A **32**, 134 (1985).

[8] A. Jain and D. W. Norcross, J. Chem. Phys. **84**, 739 (1986).

[9] F. Edard, A. P. Hitchcock, and M. J. Tronc, J. Phys. Chem. **94**, 2768 (1990).

[10] H. N. Varambhia and J. Tennyson, J. Phys. B **40**, 1211 (2007).

[11] T. N. Rescigno, B. H. Lengsfield, and C. W. McCurdy, in *Modern Electronic Structure Theory*, edited by D. R. Yarkony (World Scientific, Singapore, 1995), Vol. 1, p. 501.

[12] T. F. O'Malley, Phys. Rev. **150**, 14 (1966).

[13] C. W. McCurdy and J. L. Turner, J. Chem. Phys. **78**, 6773 (1983).

[14] G. A. Worth, M. H. Beck, A. Jäckle, and H.-D. Meyer, MCTDH package, Version 8.4, 2007; see http://www.pci.uni-heidelberg.de/tc/usr/mctdh/

[15] P. K. Pearson and H. F. Schaefer III, J. Chem. Phys. **62**, 350 (1975).

[16] J. Berkowitz, W. A. Chupka, and T. A. Walter, J. Chem. Phys. **50**, 1497 (1969).

[17] S. T. Chourou and A. E. Orel, Phys. Rev. A **77**, 042709 (2008).

[18] M. H. Beck, A. Jäckle, G. A. Worth, and H.-D. Meyer, Phys. Rep. **324**, 1 (2000).

[19] H.-D. Meyer and G. A. Worth, Theor. Chem. Acc. **109**, 251 (2003).

[20] U. V. Riss and H.-D. Meyer, J. Phys. B **26**, 4503 (1993).

[21] A. Jäckle and H.-D. Meyer, J. Chem. Phys. **105**, 6778 (1996).

[22] T. Shimanouchi, *Tables of Molecular Vibrational Frequencies Consolidated* (National Bureau of Standards, Washington, D.C., 1972), Vol. I, p. 1.

[23] D. Forney, W. E. Thompson, and M. E. Jacox, J. Chem. Phys. **97**, 1664 (1992).

[24] M. Pettersson, J. Lundell, L. Khriachtchev, and M. Rasanen, J. Chem. Phys. **109**, 618 (1998).

[25] S. T. Chourou and A. E. Orel (unpublished).

[26] J. Royal and A. E. Orel, J. Chem. Phys. **125**, 214307 (2006).

[27] O. May, J. Fedor, and M. Allan, Phys. Rev. A **80**, 012706 (2009).